


Article

Thermal-Structural Characteristics of Multi-Layer Vacuum-Insulated Pipe for the Transfer of Cryogenic Liquid Hydrogen

Jeong Hwan Kim ¹, Dae Kyeom Park ^{1,*}, Tae Jin Kim ² and Jung Kwan Seo ^{1,3,*}

¹ The Korea Ship and Offshore Research Institute, Pusan National University, Busan 46241, Korea; kjhwan1120@pusan.ac.kr

² Institute of Technology, JUNG-WOO ENE Co., Ltd., Busan 46753, Korea; rnd@cryogen.co.kr

³ Department of Naval Architecture and Ocean Engineering, Pusan National University, Busan 46241, Korea

* Correspondence: daekyeom@pusan.ac.kr (D.K.P.); seojk@pusan.ac.kr (J.K.S.)

Abstract: As the world's hydrocarbon supplies are gradually being depleted, the search for alternative energy sources with acceptably low emissions of environmentally harmful pollutants is a growing concern. Hydrogen has been proposed by numerous researchers as a fuel source for ships. Liquid hydrogen (LH₂) has been shown to be particularly attractive as a ship fuel with respect to its ability to reduce pollution, density, high performance in engines, and high caloric value per unit mass. However, working with hydrogen in the liquid phase requires very low (i.e., cryogenic) temperatures. The design of a cryogenic LH₂ pipeline is very different from the design of a normal fluid pipe due to the change between the liquid and gas states involved and the effect of thermal and structural characteristics on the cryogenic temperature during LH₂ transportation through the transfer pipeline. This study investigated the material and thermal-structural characteristics of a multi-layer vacuum-insulated pipeline system through experiments and finite element analysis. The experimental and numerical results can be used as a database of material parameters for thermal-structural analysis when designing applications such as LH₂ pipeline systems for hydrogen carriers and hydrogen-fuelled ships.

Keywords: cryogenic temperature; multi-layer vacuum insulation; liquid hydrogen; thermal-structural analysis; design parameter



Citation: Kim, J.H.; Park, D.K.; Kim, T.J.; Seo, J.K. Thermal-Structural Characteristics of Multi-Layer Vacuum-Insulated Pipe for the Transfer of Cryogenic Liquid Hydrogen. *Metals* **2022**, *12*, 549. <https://doi.org/10.3390/met12040549>

Academic Editor: Massimo Pellizzari

Received: 28 February 2022

Accepted: 21 March 2022

Published: 24 March 2022

Publisher's Note: MDPI stays neutral with regard to jurisdictional claims in published maps and institutional affiliations.



Copyright: © 2022 by the authors. Licensee MDPI, Basel, Switzerland. This article is an open access article distributed under the terms and conditions of the Creative Commons Attribution (CC BY) license (<https://creativecommons.org/licenses/by/4.0/>).

1. Introduction

As the world's hydrocarbon supplies are gradually depleted, the search for alternative energy sources is a growing concern. Hydrogen is now widely regarded as a key element of a potentially sustainable energy economy that could assist in the reduction in environmentally harmful emissions. Hydrogen has also been proposed by numerous researchers as a fuel source for ships. Liquid hydrogen (LH₂) has been shown to be an effective aircraft fuel and is particularly attractive with respect to its global producibility, ability to replace conventional fuels and thus reduce environmental emissions, ability to reduce engine noise (due to the use of hydrogen-powered electrochemical battery-propulsion systems), density, high engine performance, and high caloric value per unit mass.

However, there are a number of challenges associated with using LH₂ and/or hydrogen under standard conditions for maritime applications. For example, due to the low volumetric energy density of hydrogen under standard conditions, it is difficult to store efficiently. Attempts to solve this problem have focused on novel hydrogen storage and transfer methods, such as storage in liquefied form at cryogenic temperatures and/or bound to liquid or solid-state carriers.

LH₂ has a higher energy density than traditional hydrocarbon energy sources. In addition, when cooled to $-253\text{ }^{\circ}\text{C}$, hydrogen has a volumetric mass density of 70.8 kg m^{-3} ,

which is approximately 775 times that of gaseous hydrogen under atmospheric conditions. However, the energy density of LH₂ is only approximately 8.5 MJ/L compared with 36.3 MJ/L for diesel fuels, so greater volumes of LH₂ are required than of conventional fuels for supplying a given vehicle, even without considering the thickness of the insulation material for the LH₂ tanks. Techniques for handling LH₂ fuel were first developed and applied in aerospace programmes, and a number of conversion proposals and studies on transfer systems have been based on purely theoretical analyses or conceptual design studies under NASA contracts [1]. There is no large-scale global shipping of LH₂ in the maritime industry. Early attempts to study the trans-oceanic transport of renewable energy in the form of LH₂ were never realised [2]. However, recently, the first pilot LH₂ tanker ship was launched by Kawasaki Heavy Industries in Japan [3].

The aerospace industry remains a major player in research on the use, storage, and transfer of LH₂. The biggest challenge in LH₂ fuelling is the low temperatures at which the process must be performed to control evaporation. LH₂ storage tanks and transfer pipelines require specific insulating materials to keep heat flux as low as possible. NASA reported that 45% of the LH₂ purchased for each space shuttle launch was lost in the process chain before it reached a shuttle's fuel tank. This included a 12.6% loss during transfer from the LH₂-carrying delivery vehicles into the large onsite storage tank and a 20.6% loss during transfer from the onsite storage tank into a shuttle's fuel tank [4]. Therefore, the loss of LH₂ must be minimised to keep the overall energy efficiency of LH₂ fuelling as high as possible; however, this requires an energy-intensive liquefaction process.

Accordingly, the design of cryogenic transfer pipelines for the transport of LH₂ from storage tanks to in-ship fuel storage, such as at bunkering terminals, is a matter of urgent technological importance.

Thermal insulation is the key to minimising heat leakage in cryogenic pipelines [5]. The development of multi-layer insulation (MLI) has been the most important advance in cryogenic insulation systems in the past 50 years [6]. MLI is the best coupled insulation system and most efficient cryogenic insulation system [7]. The development of an MLI piping system of an appropriate size for a desired cryogenic flow rate is the key challenge issue, as the fluid state changes along the flow journey [8]. Studies of cryogenic insulation systems have mainly focused on the application of non-contact insulation and performance testing. However, there has been limited research into the application of multi-layer vacuum insulation (MLVI) in shipping.

In the case of stainless steel, which is generally used as a material for pipes, hydrogen has the effect of decreasing the tensile strength, the elongation to failure, the toughness or fatigue strength limit, and increasing the fatigue crack growth rate. The main risks are the delayed fracture of parts after shaping or mounting on vehicles and the cracking or unexpected fracture of an element during the use of the vehicle. Through a model-based simulation, this study investigated the thermal-structural characteristics of LH₂ transport in a cryogenic MLVI pipeline (henceforth denoted a multi-layer vacuum-insulated pipe (MVIP)) installed in LH₂-fuelled ships. The major objective was to identify the design parameters of a suitable material for multi-layer LH₂ flow, based on mechanical properties, heat balances, and pipeline structural responses, that can be used in computer-aided design engineering to study the sensitivity of the fuel transport system to arbitrarily chosen design parameters (e.g., flow rate, pipe diameter, and the thickness of the cryogenic insulation).

The underlying basis of the approach is focused on the prime criterion for an LH₂ pipeline: its ability to deliver hydrogen completely in the liquid phase to its outlet. Thus, to forestall the partial evaporation of LH₂, the temperature must remain below the saturated vapor temperature corresponding to the absolute pressure throughout the pipeline. This criterion can be met only by using stringently designed cryogenic insulation to surround an LH₂ pipe, as it is essential that the local temperature in a pipe differs by no more than 1 °C from the saturation temperature at a given local pressure. Thus, the heat balance is a critical component of our model, and the design of the pipeline system must specify precise characteristics for the components of the material and thermal-structural response. Such a

model-based simulation is the first step in the rational design of the section components of LH₂ transfer pipes.

2. Thermal-Structural Analysis Procedure for a Multi-Layer Vacuum Insulation Pipeline

2.1. Thermal-Structural Analysis Procedure

This study involved the use of methods for the thermal-structural design analysis of an MVIP in an LH₂ fuel-supply system for ships. The heat balance at cryogenic temperature and its responses were characterised by finite element (FE) analysis simulations, which were followed by analyses of heat transfer and structural responses. Figure 1 presents the procedure for the thermal-structural-based design method considered in this study.

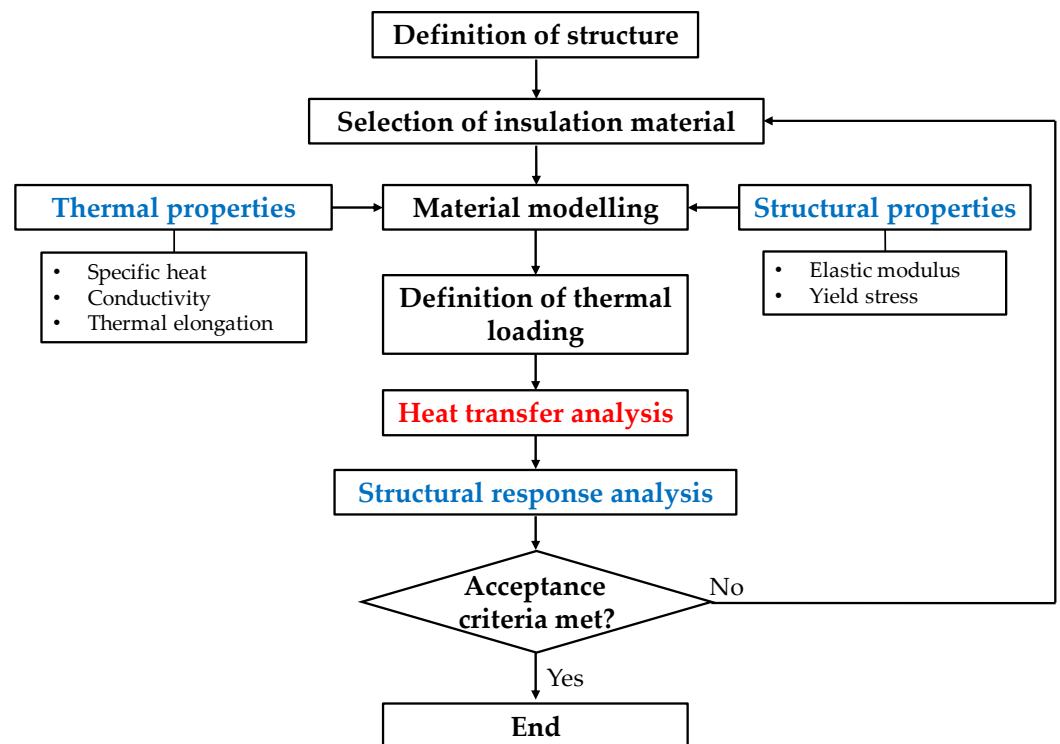


Figure 1. Flow chart of the design analysis procedure.

The procedure consisted of two parts: heat transfer and structural response analyses of the LH₂ transfer pipe. Both analyses must consider material nonlinearity to ensure accurate results. Therefore, the material properties for use in the analyses were obtained experimentally.

2.2. Multi-Layer Vacuum Insulation Pipeline

The cross-section of an LH₂ cryogenic transfer pipe with a design recommended by an industry partner is shown in Figure 2 [9]. The ambient temperature, i.e., the maximum outer pipe design temperature, is 44 °C, and the hydrogen temperature, i.e., the inner pipe design temperature, is −253 °C. A temperature gradient exists between the outer pipe and the inner pipe due to heat transfer from the former to the latter; therefore, heat flows into the pipe containing the cryogenic fluid.

The cross-section consists of cryogenic insulation film, vacuum insulation, and supporting members. Cryogenic insulation film (PF (phenolic foam) type) is the best-performing material for vacuum insulation and is widely used in cryogenic environments. Vacuum insulation is a new technique but is based on a simple principle: the core material, contained in the ‘core bag’, is compressed to approximately 200 kg/m³ density, and the internal pressure is maintained at a vacuum state of 1.0 mbar or less. Each supporting member consists of a round bar, a disc spring, and an FRP (fibre-reinforced plastic) cap, and there

are four such supporting members in each section, as shown in Figure 2a. Details of the supporting member are shown in Figure 2b.

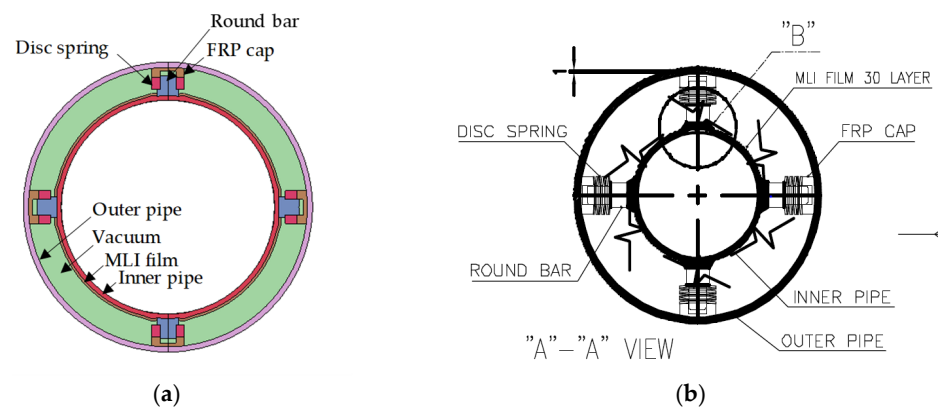


Figure 2. Multi-layer vacuum-insulated pipe (MVIP); (a) Typical cross-section of an MVIP; (b) Detail of a supporting member.

The flow-thermal and structural conditions for the modelling study were examined numerically and experimentally using the geometric configurations for which MVIP data are available. Table 1 summarises the geometrical properties of the pipe.

Table 1. Geometrical properties of the multi-layer vacuum-insulated pipe.

Type	Thickness from Inner Plate on Inner Pipe (mm)
Inner pipe	3.44
Insulation	1.82
Vacuum	19.43
Outer pipe	4.19

3. Mechanical Properties of Steel at Cryogenic Temperature

It is important to precisely define the mechanical properties for the selection of MVIP materials at cryogenic temperatures. Thus, a series of tensile tests was conducted at various temperatures, encompassing room and cryogenic temperatures, to determine the mechanical characteristics of the target materials. The tested materials included two 316-type austenitic stainless steels (316L and 316/316L) that are available for use in MVIPs. The mechanical characteristics of 316-grade stainless steel, as standardised by ASM International, were also tested.

3.1. Experimental Apparatus and Specimen Description

To investigate the material behaviour of the stainless steels in cryogenic temperature ranges, material tensile tests were performed based on tensile testing standards (ISO 6892-1: 2019 [10] at room temperature and ISO 6892-3: 2015 [11] at cryogenic temperatures). The tests were performed using a universal testing machine (Shimadzu, Kyoto, Japan) equipped with a cryogenic chamber whose interior could be cooled to -170 °C. A digital control system linked with thermocouples for generating a cryogenic environment was embedded in the cryogenic chamber. The amount of inlet liquid nitrogen was automatically controlled by the control system to maintain the temperature of the experiment. For data acquisition, a cryogenic extensometer was embedded in the specimen in the cryogenic chamber. To apply a tension load on the test specimen at cryogenic temperature, upper and lower axial loading jigs were used, with pin connections to the test specimen. Figure 3a,b show the setup of the experimental apparatus for these material tensile tests.

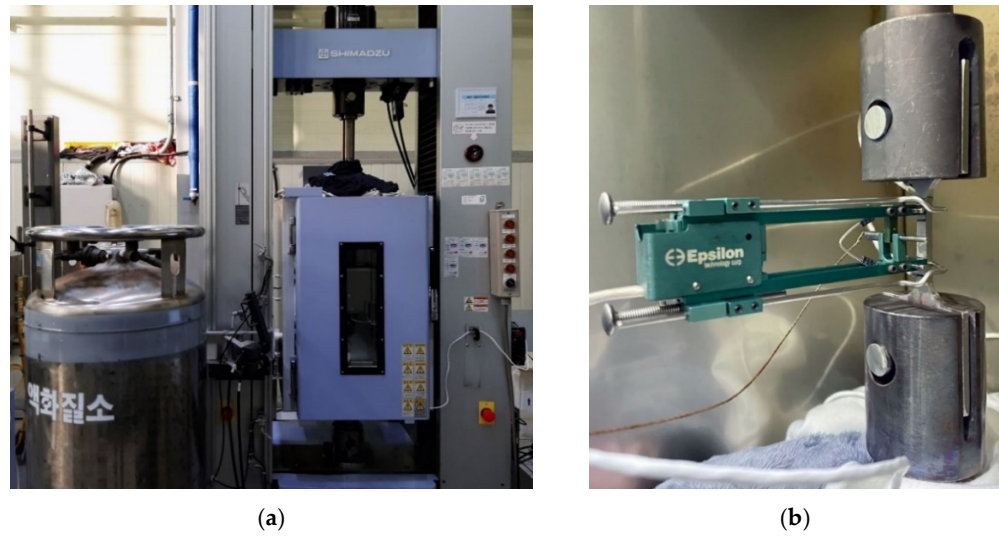


Figure 3. Experimental apparatus for tests on 316/316L steel. (a) Tensile test equipment with a cryogenic chamber; (b) test setup with a cryogenic extensometer.

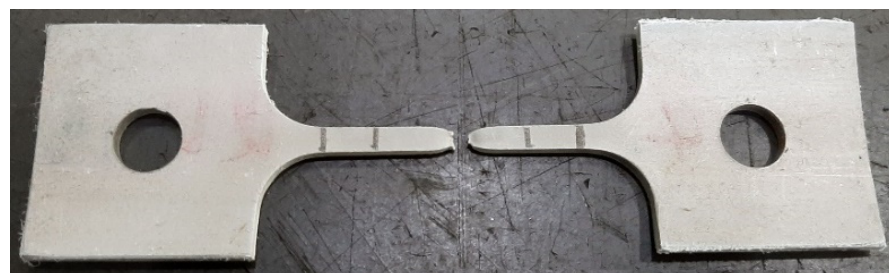
The test specimens were fabricated as plate-type dog-bone-shaped tensile specimens constructed from base members. The dimensions of the specimens are listed in Table 2. Figure 4a,b shows the test specimens of 316/316L before and after testing.

Table 2. Specific dimensions of specimens used in material tensile testing.

Material	Standard	Base Member	Width (mm)	Thickness (mm)	Gauge Length (mm)
316L	JIS G4305 [12]	Sheet	25	1.25	50
316/316L	ASTM A409M [13]	Pipe (4" 10 S) (ASME 36.16 M)	6	3.05	25



(a)



(b)

Figure 4. Test specimen of 316/316L (a) before; (b) after test.

The austenitic stainless steels, i.e., 316, 316L, and 316/316L, tested in this study are the most common materials used for the fabrication of equipment used in cryogenic conditions in the shipbuilding industry (liquefied natural gas carriers) [14]. 316/316L is a dual-grade material with the material strength of 316 but the carbon content of 316L.

Table 3 shows the chemical compositions of 316 and 316L according to the standards of JIS G4305 [12] and ASTM A409M [13]. Although 316 and 316L are both marine-grade steels, they have some key differences. Compared to 316, 316L contains a lower proportion of carbon, which cannot exceed 0.03 wt % (JIS G4305) or 0.035 wt % (ASTM A409M). This decreases the risk of carbon precipitation, making 316L a better option for welding to ensure maximum corrosion resistance.

Table 3. Elemental compositions of 316 and 316L (wt %).

Material	C Max.	Mn Max.	P Max.	S Max.	Si Max.	Ni	Cr	Mo	Standard
SUS316	0.08					10.0			JIS G4305 [12]
TP316						~14.0			ASTM A409M [13]
SUS316L	0.030	2.00	0.045	0.030	1.00	12.0	16.0~18.0	2.00~3.00	JIS G4305 [12]
TP316L	0.035					10.0			ASTM A409M [13]
						~14.0			

3.2. Experimental Results

The results of the tensile tests of the above-described steels at various temperatures were compared with ASM data [15]. The pre-determined temperatures ranged from room temperature (20 °C) to −253 °C, to encompass the temperature range typically encountered in cryogenics (room temperature to −163 °C). The results provided information on several parameters, namely yield stress, tensile stress, and fracture strain, as shown in Figure 5a–c and listed in Table 4.

The strength parameters, e.g., yield stress and tensile stress, increased linearly as the temperature decreased. However, the fracture strain showed a non-linear temperature dependence: it increased as the temperature was reduced to −40 °C but then decreased at lower temperatures. The calculated temperature dependences of these properties for 316 could not be verified due to the lack of data in the ASM.

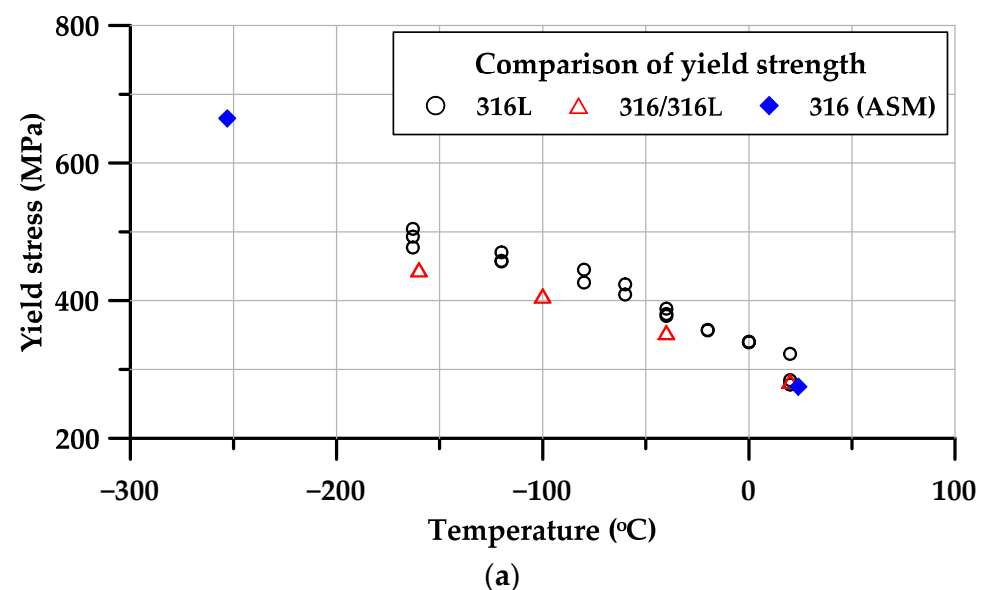


Figure 5. Cont.

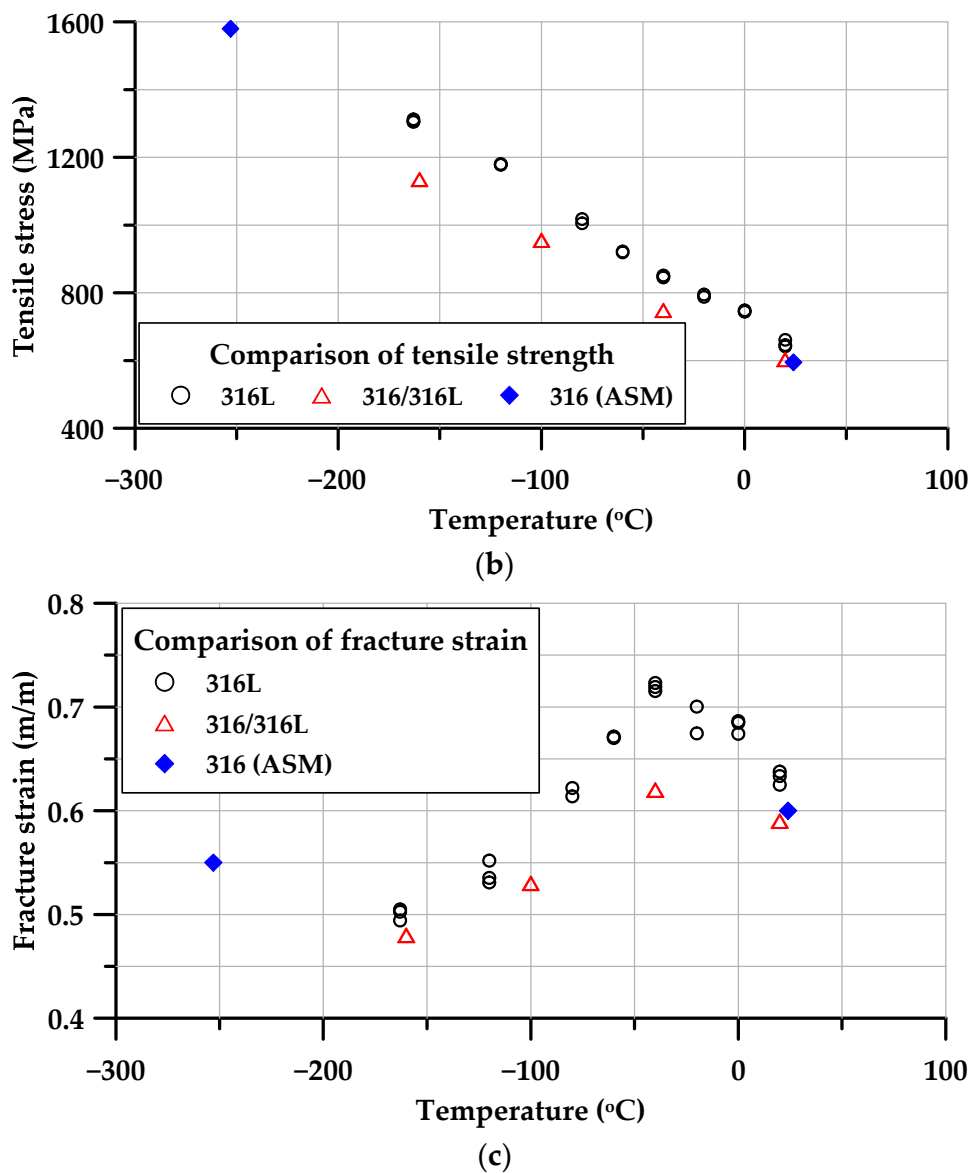


Figure 5. Mechanical characteristics vs temperature relationships of stainless steels: (a) yield strength; (b) tensile strength; (c) fracture strain.

Table 4. Tensile test results of stainless steels.

Material (Source)	Temperature (°C)	Yield Stress (MPa)		Tensile Stress (MPa)	Fracture Strain (m/m)
		Actual	Modified		
316L	20	278		642	0.64
		284	275	646	0.63
		323		661	0.63
	0	339		749	0.68
		340	320	744	0.67
		340		745	0.69
	-20	358		795	0.70
		357	337	788	0.67
		378		849	0.72
	-40	381	362	845	0.72
		388		851	0.72
	-60	409		919	0.67
		424	396	922	0.67

Table 4. Cont.

Material (Source)	Temperature (°C)	Yield Stress (MPa)		Tensile Stress (MPa)	Fracture Strain (m/m)
		Actual	Modified		
316/316L	−80	445	416	1018	0.61
		426		1005	0.62
		457		1178	0.55
	−120	470	442	1181	0.53
		458		1179	0.54
		477		1307	0.50
	−163	504	472	1312	0.50
		493		1305	0.49
20	283	275	603	0.59	
316 (ASM)	−40	354	346	748	0.62
	−100	407	399	955	0.53
	−160	445	437	1135	0.48
316 (ASM)	24	275	595	0.60	
	−253	665	1580	0.55	

3.3. Material Model

To develop an elastic–perfectly plastic material model for the following thermal–structural numerical analysis, a formula for yield-stress curve prediction was derived from the modified yield stress vs. temperature relationship in Figure 6. Modifications of the test results were carried out to obtain the same yield stress at room temperature as a baseline. In total, 21 test results on 316L at 8 different temperatures were averaged and counterbalanced the yield strength of ASM at room temperature (275 MPa). The same procedure was performed on the test results on 316/316L. The modified yield stresses are listed in Table 4 and plotted in Figure 6.

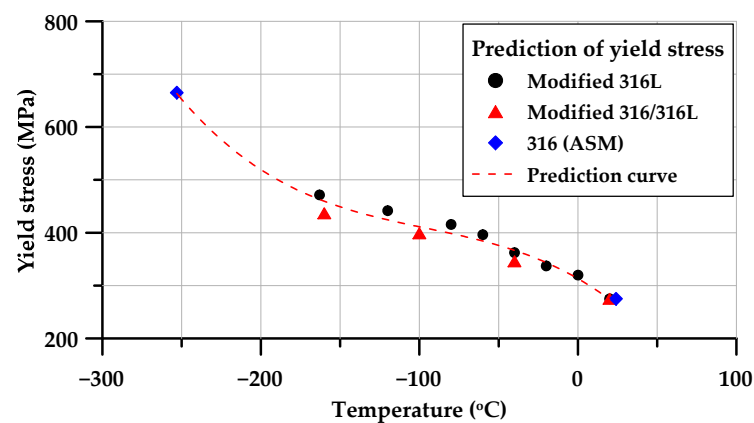


Figure 6. Yield stress prediction model of 316-type stainless steels for numerical analysis.

From the yield stress vs. temperature data of the modified 316-type steels, a cubic formula, Equation (1), was derived to accurately predict the yield stress vs. temperature behaviours of 316-type steels. A piecewise linear material model is used with the yield-stress prediction formula in the numerical analyses.

$$\text{Yield stress at } T \text{ (}^\circ\text{C)} = a + b \cdot T + c \cdot T^2 + d \cdot T^3 \quad (1)$$

where $a = 3.15 \times 10^2$, $b = -1.73 \times 10^0$, $c = -1.15 \times 10^{-2}$, and $d = -4.02 \times 10^{-5}$.

4. Numerical Investigation

4.1. Heat-Transfer Analysis under Cryogenic Conditions

Heat transfer processes under cryogenic conditions and the analysis of their application are fundamentally very similar to those under general high-temperature (flame temperature) conditions. The three heat-transfer mechanisms (conduction, convection, and radiation) that take place at ambient temperatures or higher also occur in the cryogenic temperature range. To study the changes in properties of the various phases in a pipeline, all of the general heat-transfer equations can be applied to the cryogenic temperature range. In this study, it was assumed that the prime criterion for an LH₂ pipe is its ability to deliver entirely liquid-phase hydrogen to its outlet. Therefore, only the physical state of the hydrogen flow and the heat transfer processes in the target MVIP need be considered.

4.1.1. Modelling of Heat Transfer Analysis

To perform heat transfer and structural-response analysis, the target MVIP was modelled by FE analysis using a commercial FE code (LS-DYNA) [16] as shown in the Figure 7. A total of 74,808 solid elements were used to perform the heat transfer analysis in the thickness direction. The applied material properties comprised the mechanical properties obtained from experimental results on the current study and the thermal properties, namely the specific heat, thermal conductivity coefficient, and thermal expansion coefficient, which were obtained from a database [15]. The thermal properties used for the thermal analyses are listed in Table 5.

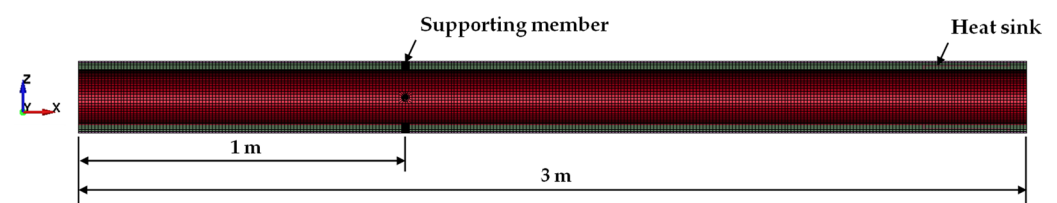


Figure 7. Finite element model of MVIP.

Table 5. Thermal properties of MVIP.

Type	Specific Heat (J/kg·K)	Thermal Conductivity (W/mK)	Thermal Expansion Coefficient
Pipe (TP316L)	500	14.6	1.28×10^{-5}
MLI film	800	0.000135	-
Vacuum	1006	0.0001	-
Heat sink (SUS F304)	500	14.6	1.37×10^{-5}
Support cap (FRP)	787	1.1	3.53×10^{-5}

4.1.2. Analysis Procedure

In the heat transfer analysis, it was assumed that the initial temperature of the transfer pipe was 20 °C. The analysis was divided into three parts (Figure 8), as shown below.

- Heat transfer between LH₂ and the inner pipe: it was assumed that the surface of the inner pipe in contact with LH₂ had the same temperature as the LH₂.
- Heat transfer between the inner pipes: the temperature was calculated according to the thickness of pipe and the insulation, using the thermal conductivity coefficient of the pipe and the insulation.
- Heat transfer between the outer pipe and the external environment (ambient temperature): it was assumed that the surface of the outer pipe in contact with the external environment had the same temperature as the ambient air.

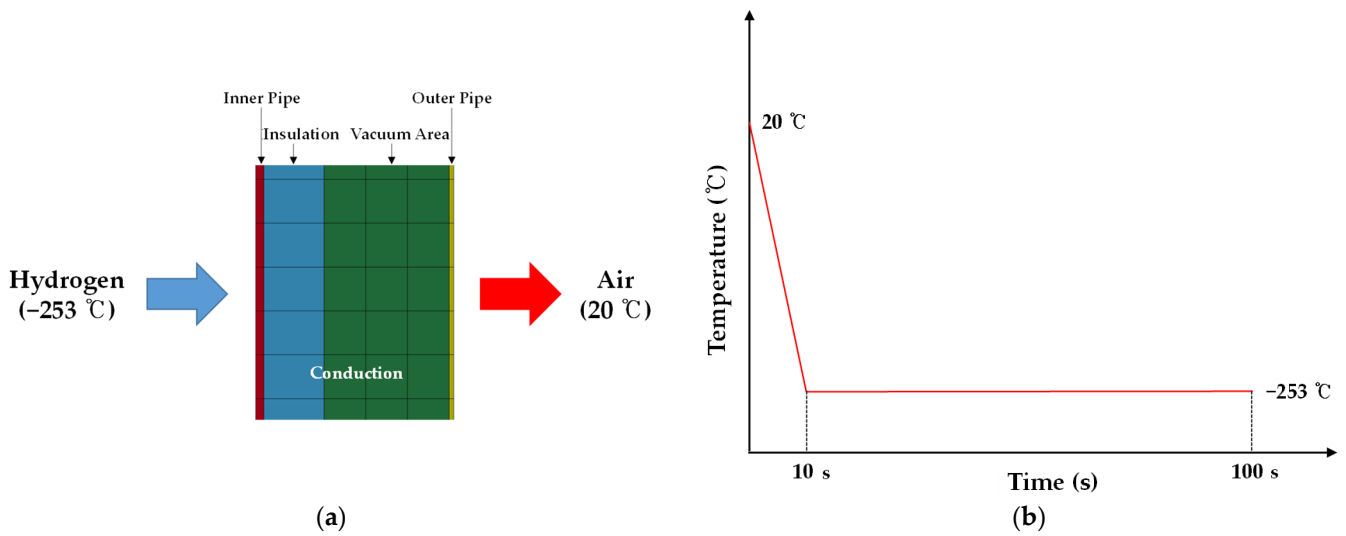


Figure 8. Procedure of heat transfer analysis. (a) Schematic of process of heat-transfer analysis of MVIP; (b) thermal-loading profile of LH₂.

4.1.3. Results of Heat Transfer Analysis

Heat transfer analysis of an MVIP was conducted to quantify its insulation performance and thus provide insights for design parameter selection. LH₂ injection was assumed to take place within 10 s, and a load was applied to the inner surface of the transfer pipe in a temperature-dependent manner. Figures 9 and 10 show the steel temperature-distribution of the heat sink and inner supporting member of the MVIP at various times. Figure 11 plots the steel temperature versus time at various positions on the supporting member.

The results of the analysis confirmed that heat transfer through the MLI and vacuum part was minimal, and that heat conduction mainly occurred on the inner surface of the LH₂ transfer pipe through the internal support and heat sink.

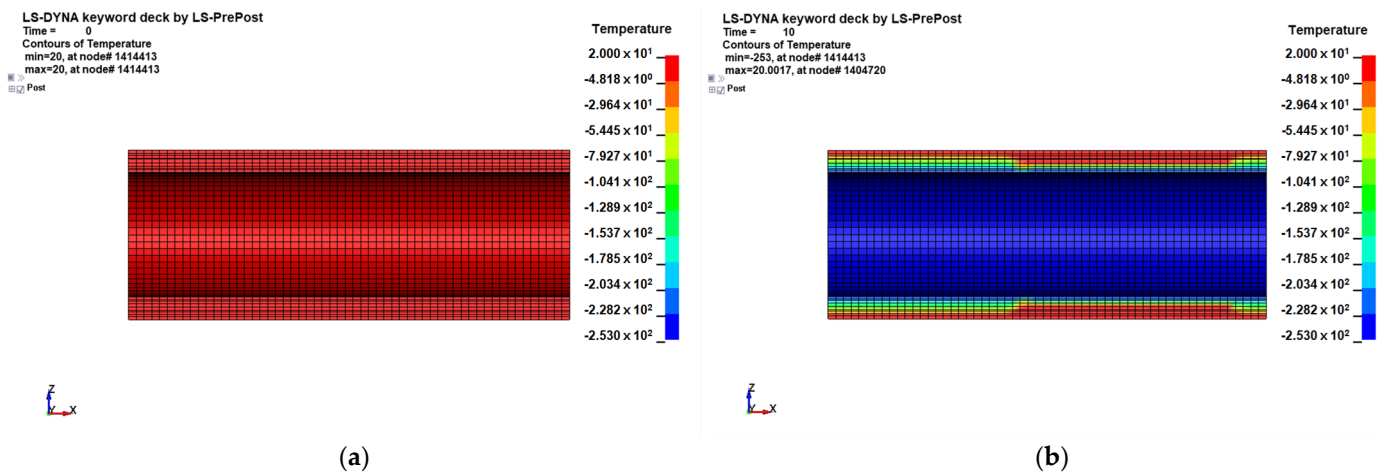


Figure 9. Cont.

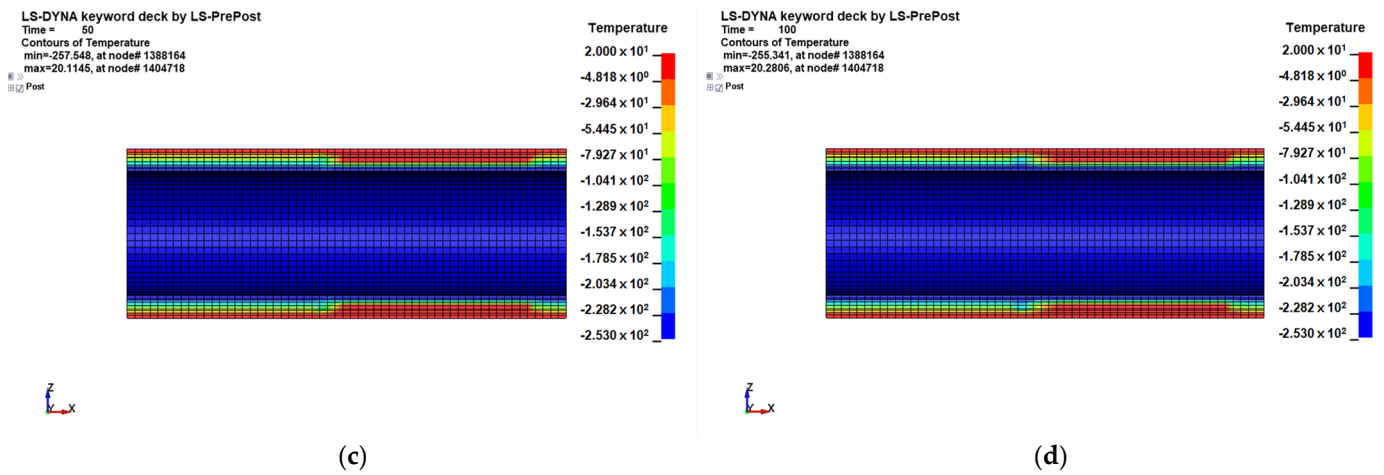


Figure 9. Steel temperature calculated in the heat sink part of the MVIP; (a) 0 s; (b) 10 s; (c) 50 s; (d) 100 s.

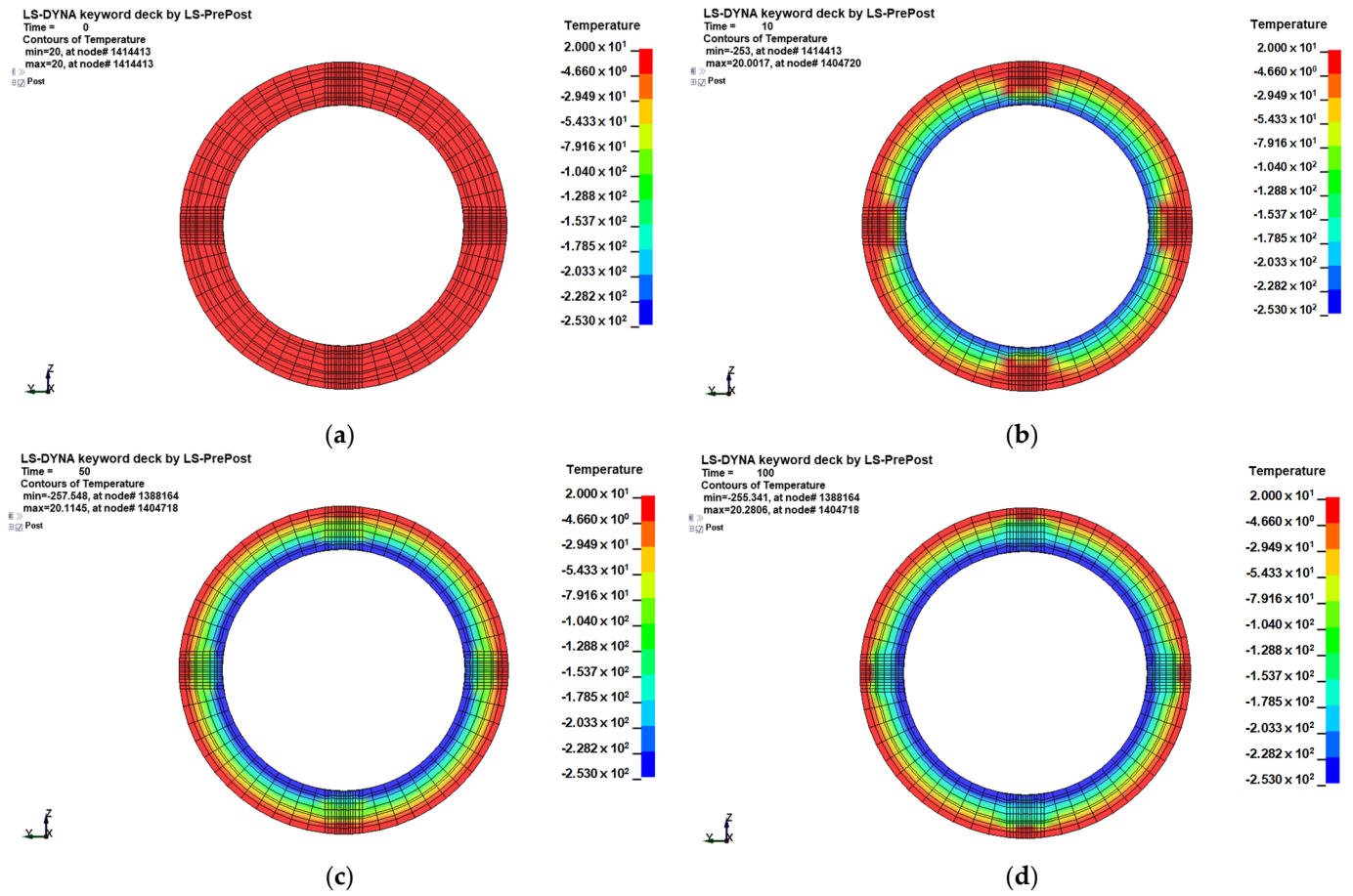


Figure 10. Steel temperature calculated in the inner supporting member of the MVIP; (a) 0 s; (b) 10 s; (c) 50 s; (d) 100 s.

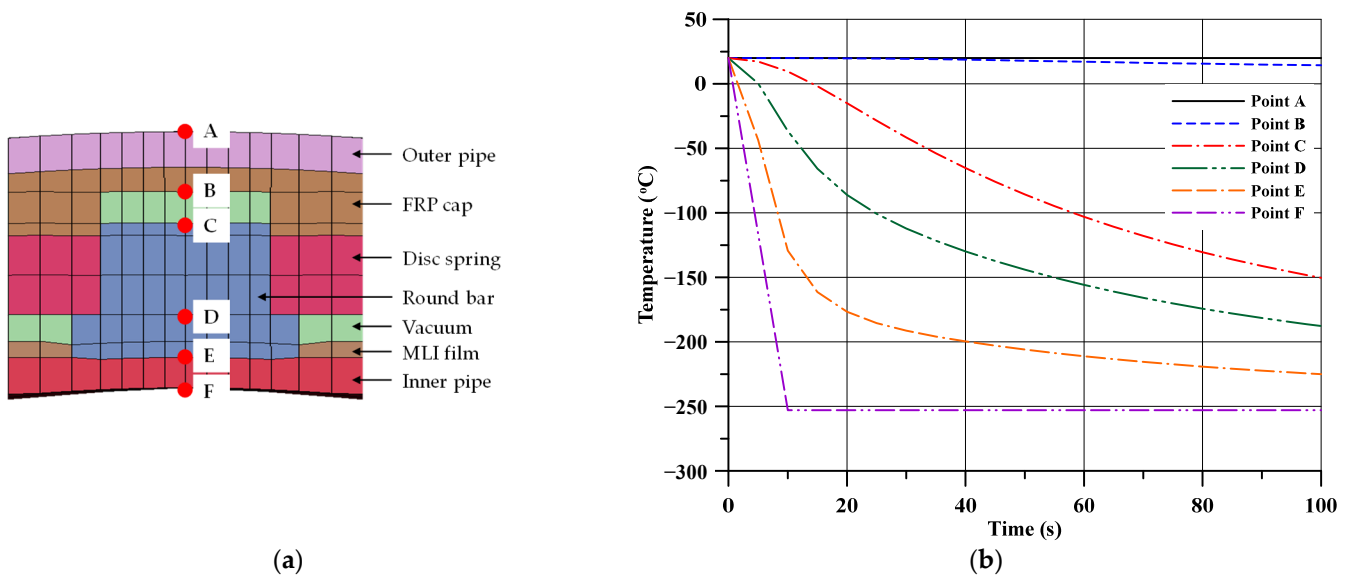


Figure 11. Steel temperature of the supporting member calculated at six points. (a) Temperature-measurement points on a supporting member; (b) steel temperature versus time at measurement points.

4.2. Structural Response Analysis under Cryogenic Conditions

4.2.1. Methodology of Structural Response Analysis

A series of non-linear FE analyses of heat transfer at various low temperatures was performed to investigate the structural behaviour of the MVIP. LH₂ injection was assumed to take place within 10 s, and a load was applied to the inner surface of the transfer pipe in a temperature-dependent manner. MLI films and vacuum components were not included in the structural response analysis because they are not structural members. Figure 12 shows the configuration of the FE model of the MVIP used for structural response analysis. Structural response analysis was performed by dividing the inner supporting member of the pipe into sections at intervals of 2 m, 3 m, or 4 m, to identify the effect of the interval length (henceforth denoted the ‘inner support interval’), as shown in Figure 13.

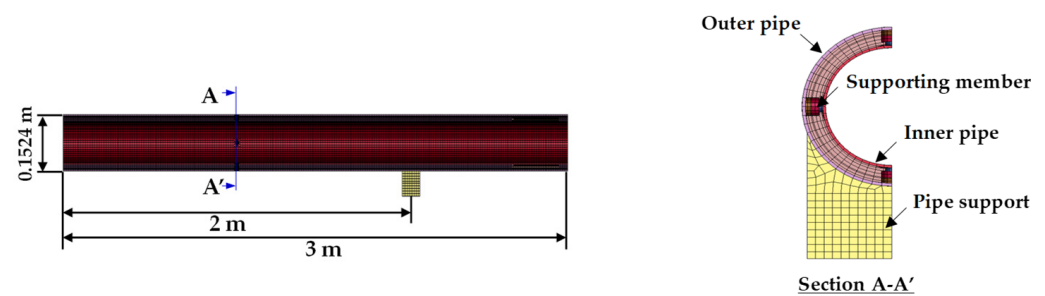


Figure 12. FE model of MVIP for structural response analysis.

Figure 14 and Table 6 show the boundary conditions for structural response analysis. The thermal load was the same as in the heat transfer analysis, while for the mechanical load, only the self-weight was considered. A database of the thermal and mechanical properties of the MVIP was built from the tensile test results (Table 7) and ASM Specialty Handbook: Stainless Steels [15].

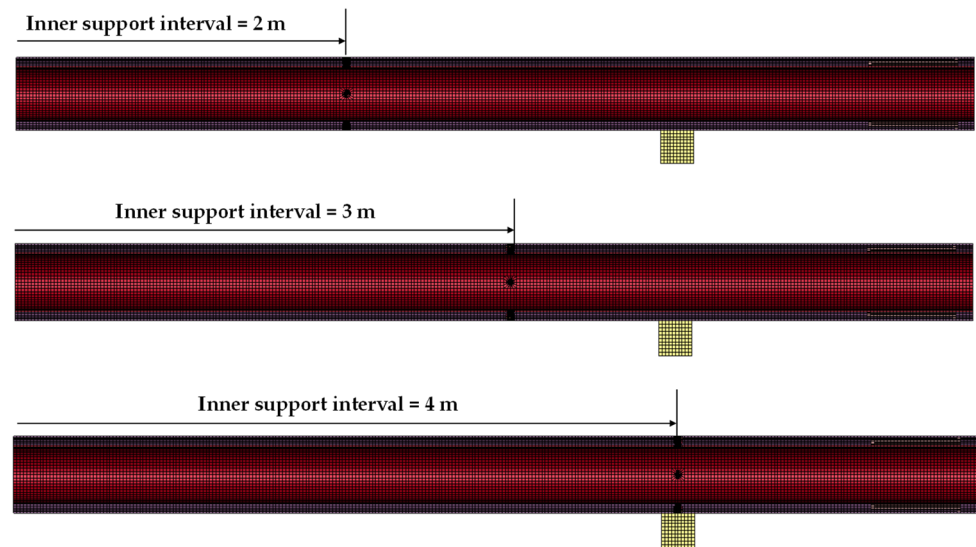


Figure 13. FE models with various interval lengths for sectioning of the inner supporting member.

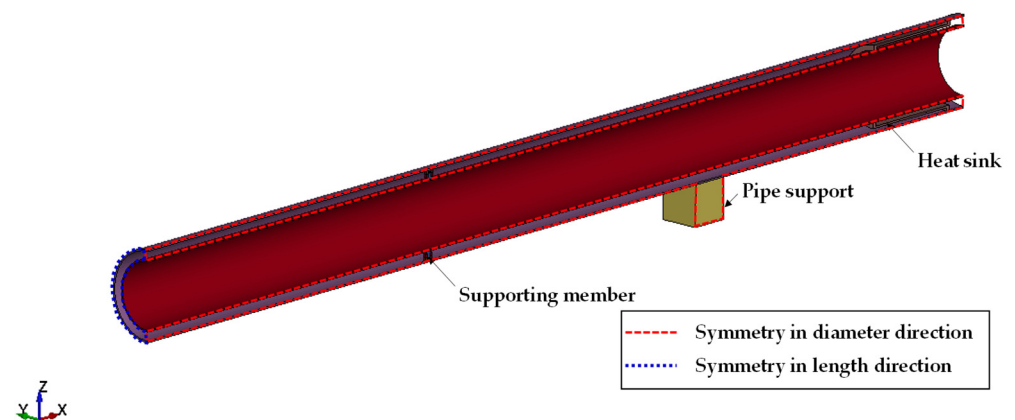


Figure 14. Boundary conditions for structural response analysis.

Table 6. Boundary conditions (U = translational degree of freedom, R = rotational degree of freedom).

Part	Description *
Bottom surface of pipe support	$U_x, U_y, U_z = 1$ and $R_x, R_y, R_z = 0$
Edges in the y -direction	$U_y = 1$ and $U_x, U_z, R_x, R_y, R_z = 0$
Edges in the x -direction	$U_x = 1$ and $U_y, U_z, R_x, R_y, R_z = 0$

* 1 indicates that there is a translational constraint; 0 indicates that there is no translational constraint.

Table 7. Mechanical properties of MVIP.

Component	Temperature (°C)	Density (kg/m ³)	Elastic Modulus (MPa)	Yield Stress (from Equation (1)) (MPa)	Poisson's Ratio
Pipe (TP316L)	20	7900	19,300	275	0.3
	0			315	
	−40			368	
	−80			400	
	−120			426	
	−160			462	
	−210			543	
−260	694				
Heat sink (SUS F304)	20	7900	19,300	295	0.3
Support cap	20	2560	6890	331	0.276

4.2.2. Results of Structural Response Analysis

Figure 15 shows the deformed shape of the MVIP with various inner support intervals after 100 s, and Figure 16 shows the displacement results at the centre of the inner supporting member of the MVIP with various inner support intervals. It can be confirmed that the displacement changes while liquid hydrogen is injected and the displacement is maintained thereafter. The greatest maximum deflection was 0.0127 m, which was obtained in the case with an inner support interval of 4 m. From the displacement result, it can be seen that the gap between the inner pipe and the outer pipe decreases as the inner support interval increases. Figures 17 and 18 show the von Mises stress and plastic strain distribution at different inner support intervals. Table 8 summarises the results of the structural response analysis of the MVIP, namely the deflection, von Mises stress, and plastic strain.

The results of the structural response analysis confirmed that the inner support interval affected the structural behaviour. In particular, in the case of a 4 m inner support interval, the inner supporting member was severely deformed, as shown in Figure 19.

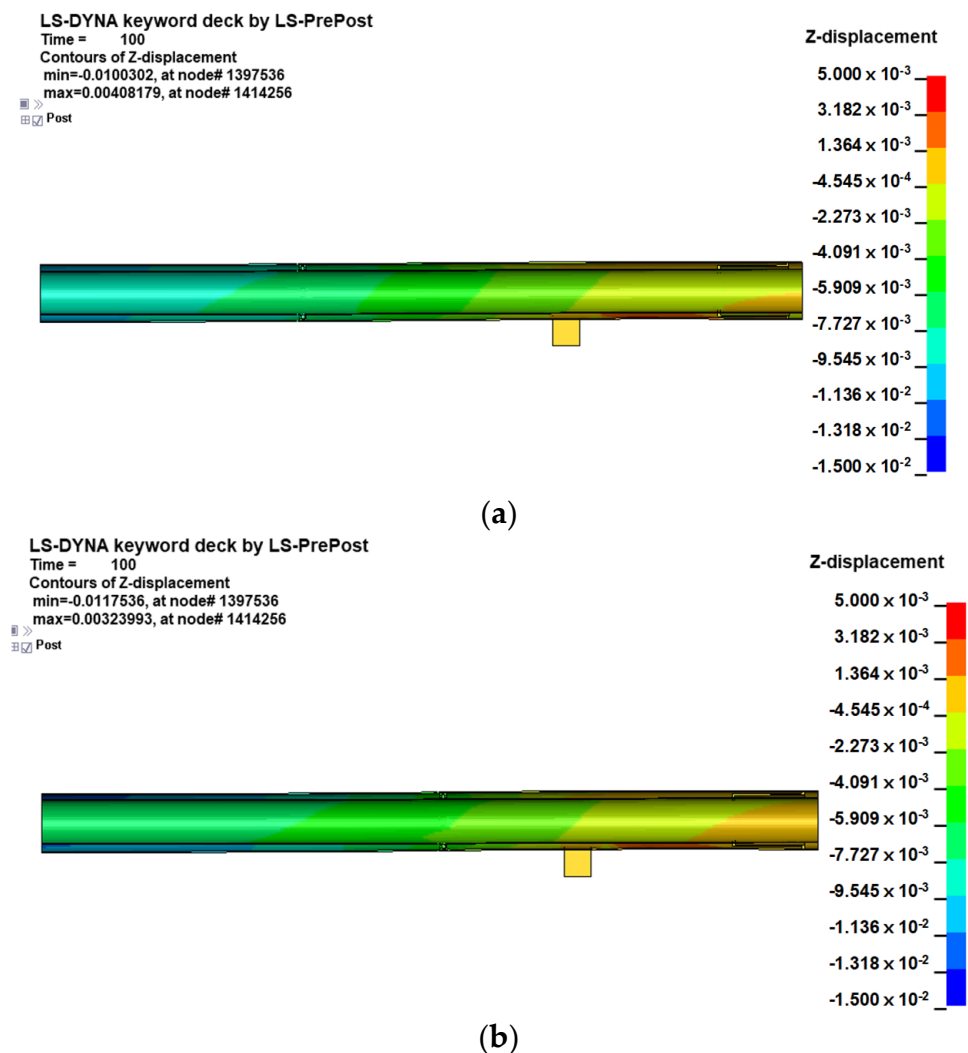


Figure 15. Cont.

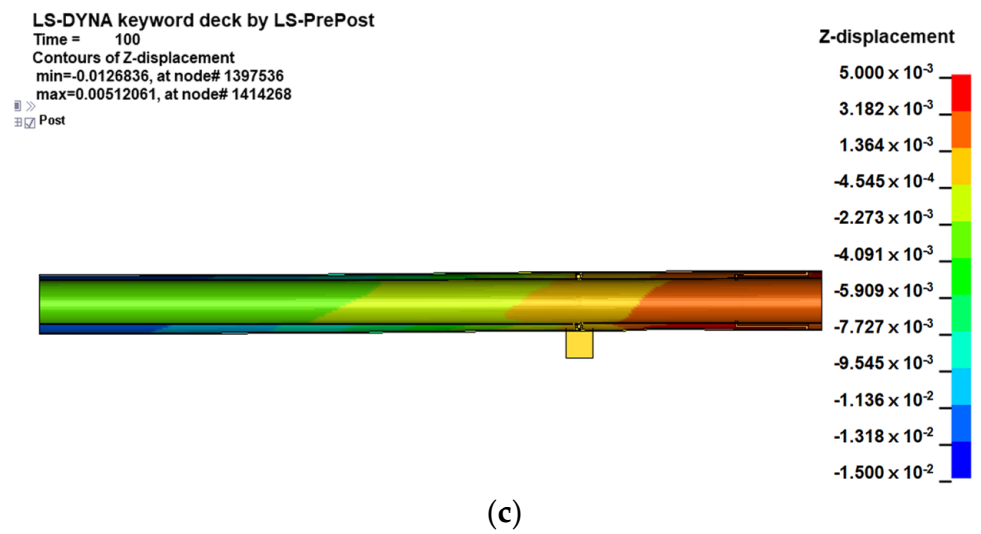


Figure 15. Deformed shape of an MVIP with various inner support intervals after 100 s; (a) Interval = 2 m (maximum deflection = 0.0100 m); (b) Interval = 3 m (maximum deflection = 0.0118 m); (c) Interval = 4 m (maximum deflection = 0.0127 m).

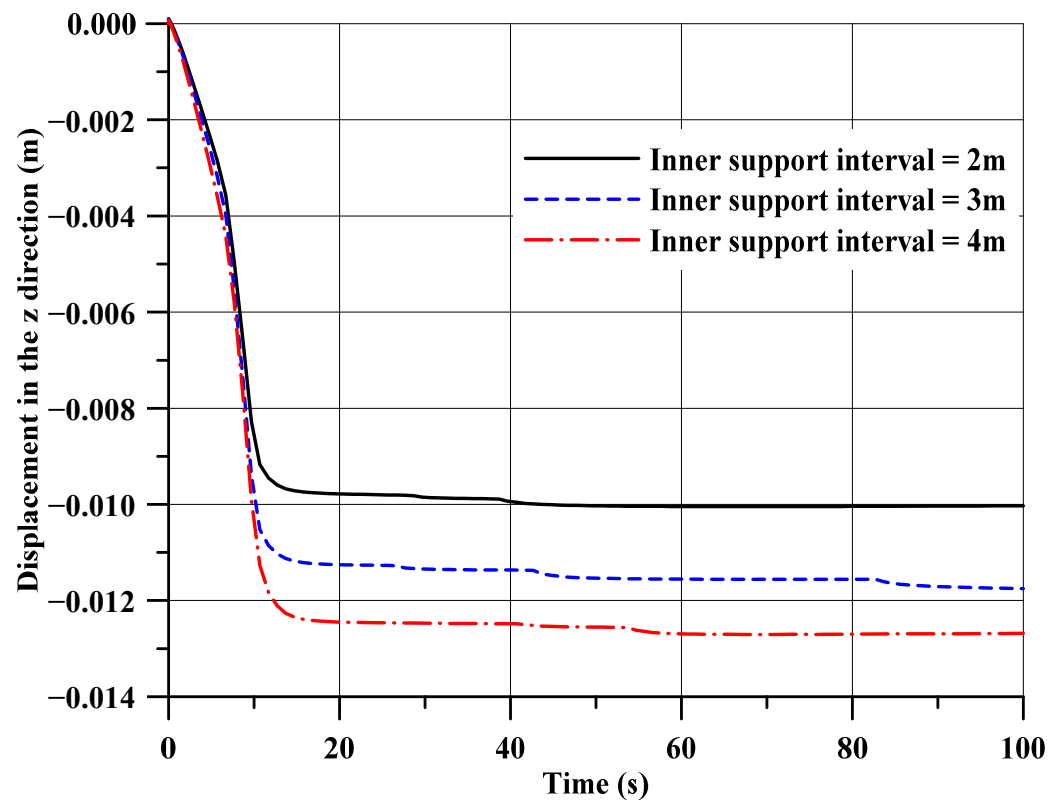
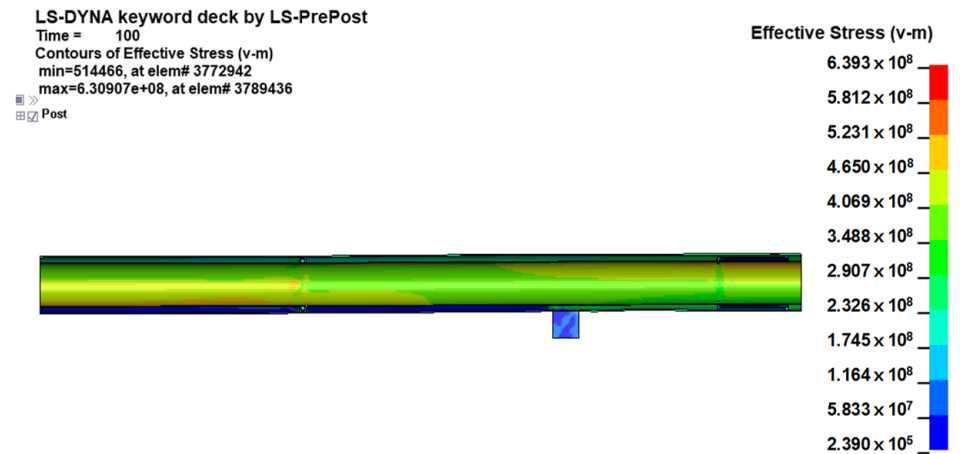
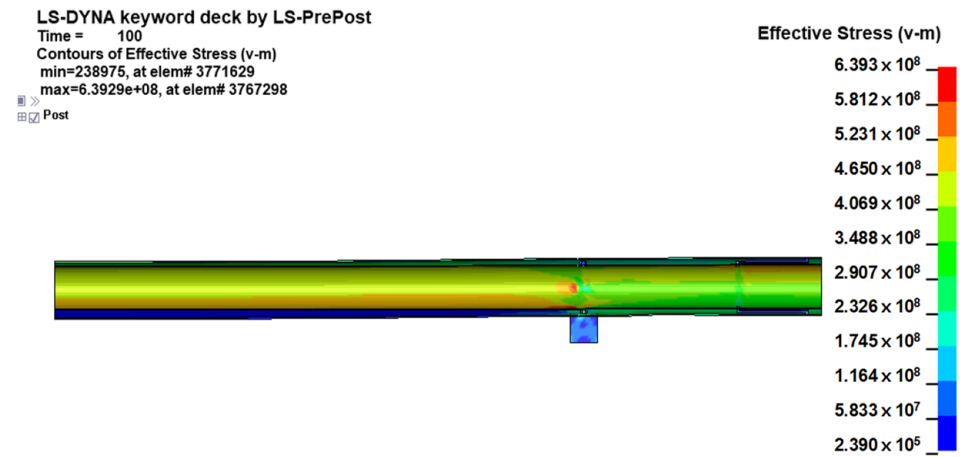


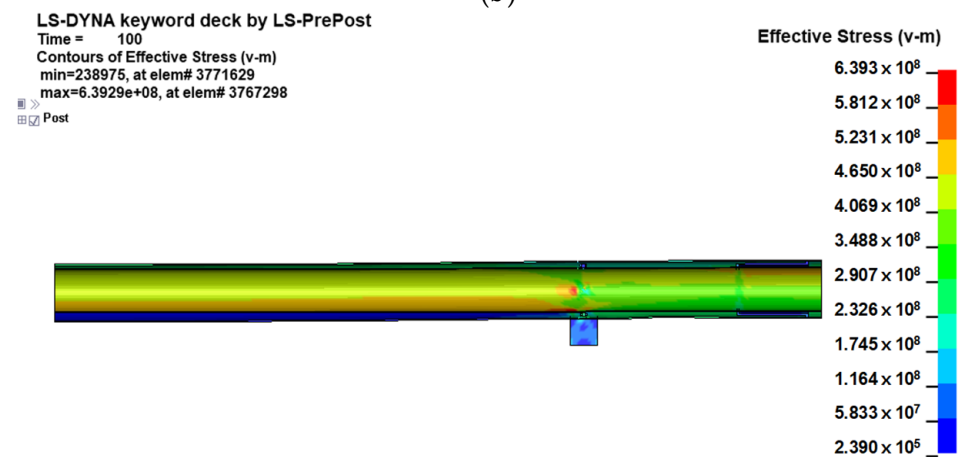
Figure 16. Displacement results at the centre of the inner support of MVIP with various inner support intervals.



(a)



(b)



(c)

Figure 17. von Mises stress distribution of MVIP with various inner support intervals after 100 s; (a) Interval = 2 m (maximum von Mises stress = 631 MPa); (b) Interval = 3 m (maximum von Mises stress = 649 MPa); (c) Interval = 4 m (maximum von Mises stress = 639 MPa).

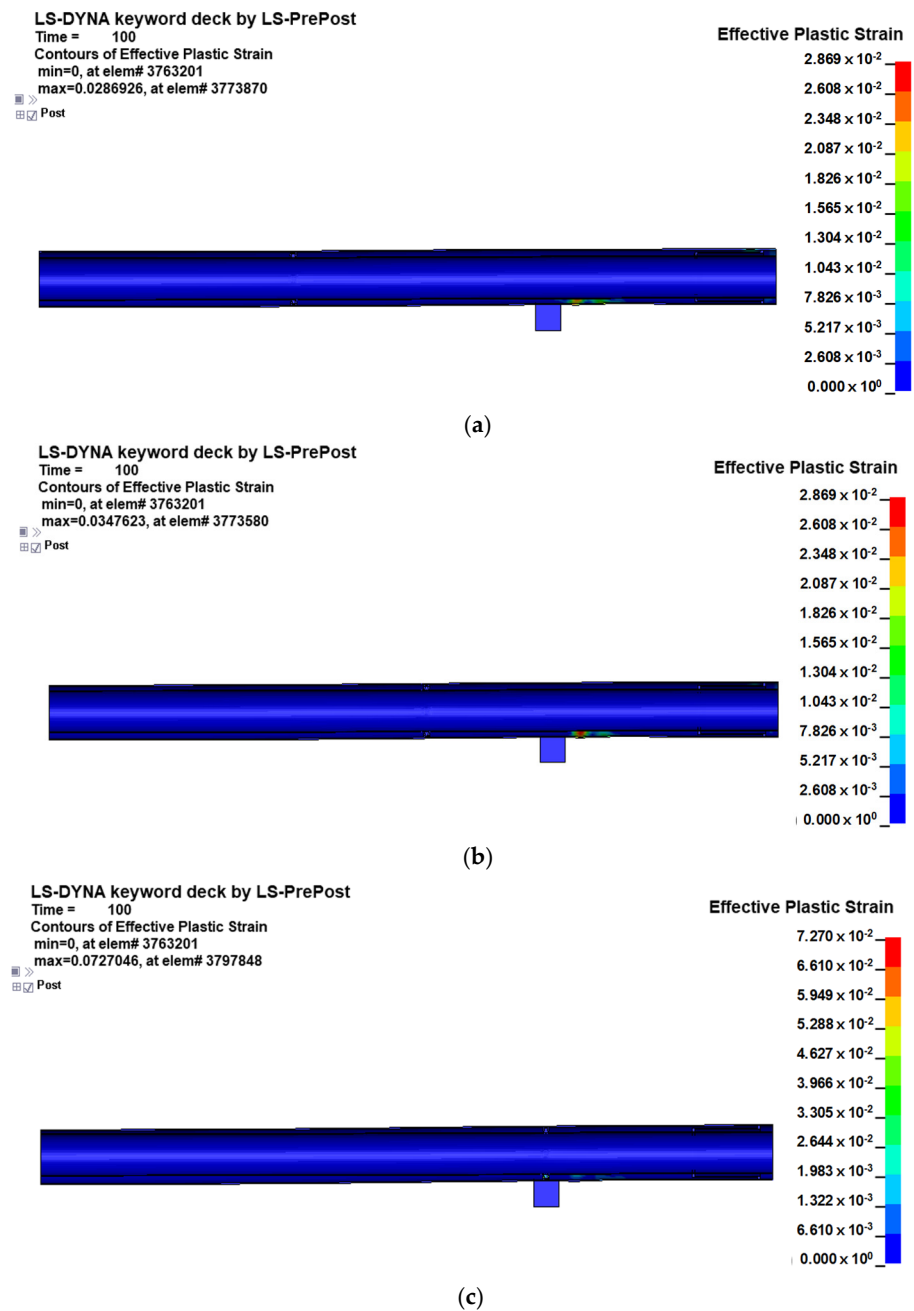


Figure 18. Plastic strain distribution of MVIP with various inner support intervals after 100 s; (a) Interval = 2 m (maximum plastic strain = 0.0287); (b) Interval = 3 m (maximum plastic strain = 0.0348); (c) Interval = 4 m (maximum plastic strain = 0.0727).

Table 8. Summary of structural response analysis results.

Inner Support Interval	Maximum Value		
	Deflection (m)	Von Mises Stress (MPa)	Plastic Strain
2 m	0.0100	631	0.0287
3 m	0.0118	649	0.0348
4 m	0.0127	639	0.0727

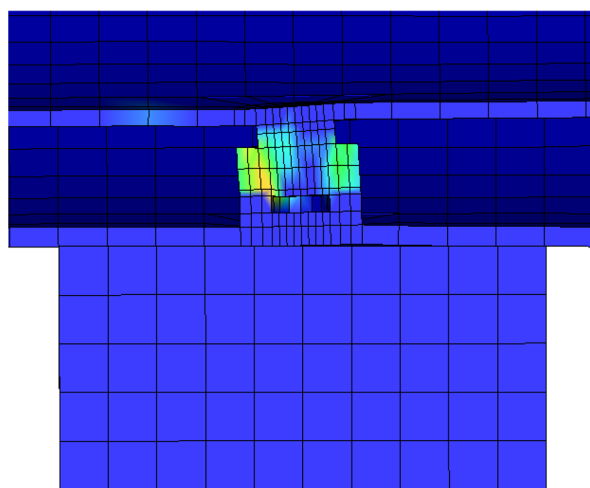


Figure 19. Deformed shape of inner supporting member (inner support interval = 4 m).

5. Conclusions

This study performed model-based simulations to investigate the thermal-structural characteristics of LH₂ transport in a pipeline installed in LH₂-fuelled ships with a cryogenic MVIP. The major objective was to identify the design parameters of a suitable material for multi-layer LH₂ flow, based on the mechanical properties, heat balances, and pipeline structural responses. These would be useful for use in computer-aided design engineering studies of the sensitivity of an LH₂ transport system to arbitrarily chosen design parameters (e.g., flow rate, pipe diameter, and thickness of the cryogenic insulation).

Based on the results of this study, the following conclusions and insights can be drawn.

1. Thermal-structural design analysis methods were applied for examining an MVIP in an LH₂ fuel-supply system for ships. These analysis methods can be useful for the design of an MVIP.
2. A series of tensile tests was conducted at various temperatures, encompassing room and cryogenic temperatures, to understand the mechanical characteristics of the target materials. From the results, a formula for yield-stress curve prediction was derived, incorporating a modified yield stress vs. temperature relationship.
3. When performing heat transfer and structural response analyses of MVIPs, the dependence of thermal and mechanical properties on cryogenic temperatures should be considered. In this study, the mechanical properties obtained through tensile tests were used.
4. The results of heat transfer analysis confirmed that heat is transmitted through the inner supporting member, and the insulation of the inner supporting member should be considered in the pipe design.

A series of nonlinear FE analyses was performed under various low-temperature conditions, using the results of the heat transfer analyses, to investigate the structural response of MVIPs. The results confirmed that the interval length of the sections into which the inner supporting member is divided is an important variable, and the external pipe-support interval should also be considered.

When designing an MVIP, it is necessary to consider the effects of the cryogenic temperature, the performance of the insulation, and the shape and section length of the inner pipe. In a follow-up to this study, the performance of a designed MVIP will be tested to verify the numerical analysis method in comparison with other analysis methods.

Author Contributions: Conceptualisation, J.H.K. and D.K.P.; methodology, J.H.K., D.K.P. and J.K.S.; software, J.H.K.; validation, T.J.K., D.K.P. and J.K.S.; formal analysis, J.H.K.; investigation, D.K.P. and T.J.K.; resources, T.J.K.; data curation, D.K.P.; writing—original draft preparation, J.K.S.; writing—review and editing, J.H.K. and D.K.P.; visualisation, J.H.K.; supervision, J.K.S.; project

administration, J.H.K. and J.K.S.; funding acquisition, J.H.K. All authors have read and agreed to the published version of the manuscript.

Funding: This work was supported by the Korea Agency for Infrastructure Technology Advancement (KAIA) grant funded by the Ministry of Land, Infrastructure and Transport (Grant 20TBIP-C155837-02).

Institutional Review Board Statement: Not applicable.

Informed Consent Statement: Not applicable.

Data Availability Statement: The data presented in this study are available on request from the corresponding author.

Conflicts of Interest: The authors declare no conflict of interest.

References

1. Brewer, G.D. *LH2 Airport Requirements Study*; Lockheed: Burbank, CA, USA, 1976.
2. Gretz, J.; Baselt, J.P.; Ullmann, O.; Wendt, H. The 100 MW Euro-Quebec hydro-hydrogen pilot project. *Int. J. Hydrogen Energy* **1990**, *15*, 419–424.
3. Kamiya, S.; Nishimura, M.; Harada, E. Study on introduction of CO₂ free energy to Japan with liquid hydrogen. *Phys. Procedia* **2015**, *67*, 11–19.
4. Partridge, J.K. Fractional consumption of liquid hydrogen and liquid oxygen during the space shuttle program. *AIP Conf. Proc.* **2012**, *1434*, 1765–1770.
5. Lyea, L.C.; Adama, N.M.; Ahmad, K.A. Cryogenic pipe flow simulation for liquid nitrogen with vacuum insulated pipe (VIP) and polyurethane (PU) foam insulation under steady-state conditions. *Therm. Sci. Eng. Prog.* **2018**, *7*, 302–310.
6. Timmerhaus, K.D. *Cryogenic Engineering: Fifty Years of Progress*; Springer: New York, NY, USA, 2007; pp. 120–133.
7. Chorowski, M.; Polinski, J. Modeling of multilayer vacuum insulation—Complexity versus accuracy. In Proceedings of the Twentieth International Cryogenic Engineering Conference (ICEC20), Beijing, China, 11–14 May 2004; pp. 793–796.
8. Krishnamurthy, M.; Chandra, R.; Jacob, S.; Kasthuriangan, S.; Karunanithi, R. Experimental studies on cool-down and mass flow characteristics of a demountable liquid nitrogen transfer line. *Cryogenics* **1996**, *36*, 435–441.
9. JUNG-WOO ENE Co., Ltd. Available online: <https://fgss.co.kr/> (accessed on 27 December 2021).
10. *ISO/Technical Committee 164/SC 1; Metallic Materials—Tensile Testing—Part 1: Method of Test at Room Temperature EN ISO 6892-1:2019*. International Organization for Standardization: Geneva, Switzerland, 2019.
11. *ISO/Technical Committee 164/SC 1; Metallic Materials—Tensile Testing—Part 3: Method of Test at Low Temperature EN ISO 6892-3:2015*. International Organization for Standardization: Geneva, Switzerland, 2015.
12. *JIS G4305:2012; Cold-rolled Stainless Steel Plate, Sheet and Strip*. Japanese Standards Association (JISC): Tokyo, Japan, 2012.
13. American Society for Testing and Materials (ASTM) International. Standard Specification for Welded Large Diameter Austenitic Steel Pipe for Corrosive or High-Temperature Service. ASTM A409/A409M-19. In *Annual Book of ASTM Standards*; ASTM International: West Conshohocken, PA, USA, 2019.
14. Fultz, B.S. The Challenges of LNG Materials Selection. In Proceedings of the Annual Conference of the Australasian Corrosion Association 2014: Corrosion and Prevention, Darwin, Australia, 21–24 September 2014; pp. 1–14.
15. Davis, J.R. (Ed.) *Stainless Steels*; ASM International: Almere, The Netherlands, 2010.
16. Hallquist, J.O. *LS-DYNA Keyword User's Manual*; Livermore Software Technology Corporation R11: Livermore, CA, USA, 2021.